Charged Pion Production in ν_μ Interactions on Hydrocarbon at $\langle E_\nu \rangle$= 4.0 GeV

B. Eberly,[1,*] L. Aliaga,[2,3] O. Altinok,[4] M.G. Barrios Sazo,[5] M. Betancourt,[6] A. Bodek,[7] A. Bravar,[8] H. Budd,[7] A. Butkevich,[9] D.A. Martinez Caicedo,[10,6] M.E. Christy,[11] J. Chvojka,[7] H. da Motta,[10] M. Datta,[11] J. Devan,[2] S.A. Dytman,[1] G.A. Díaz,[3] J. Felix,[5] L. Fields,[12] R. Fine,[7] A.M. Gago,[3] H. Gallagher,[4] R. Gran,[13] D.A. Harris,[6] A. Higuera,[7,5] K. Hurtado,[10,14] T. Kafka,[4] M. Kordosky,[2] T. Le,[15] E. Maher,[16] S. Manly,[7] W.A. Mann,[4] C.M. Marshall,[7] K.S. McFarland,[7,6] C.L. McGivern,[1] A.M. McGowan,[7] J. Miller,[17] A. Mislivec,[7] J.G. Morfín,[6] J. Mousseau,[18] T. Muhlbeier,[10] D. Naples,[1] J.K. Nelson,[2] A. Norrick,[2] J. Osta,[6] J.L. Palomino,[10] V. Paolone,[1] J. Park,[7] C.E. Patrick,[12] G.N. Perdue,[6,7] L. Rakotondravohitra,[6,†] R.D. Ransome,[15] H. Ray,[18] L. Ren,[1] P.A. Rodrigues,[7] H. Schellman,[12] D.W. Schmitz,[19,6] C. Simon,[20] J.T. Sobczyk,[6,‡] C.J. Solano Salinas,[14] N. Tagg,[21] B.G. Tice,[15,§] T. Walton,[11] J. Wolcott,[7] M.Wospakrik,[18] G. Zavala,[5] and D. Zhang[2]

(MINERvA Collaboration)

[1] *Department of Physics and Astronomy, University of Pittsburgh, Pittsburgh, Pennsylvania 15260, USA*
[2] *Department of Physics, College of William & Mary, Williamsburg, Virginia 23187, USA*
[3] *Sección Física, Departamento de Ciencias, Pontificia Universidad Católica del Perú, Apartado 1761, Lima, Perú*
[4] *Physics Department, Tufts University, Medford, Massachusetts 02155, USA*
[5] *Campus León y Campus Guanajuato, Universidad de Guanajuato, Lascurain de Retana No. 5, Col. Centro. Guanajuato 36000, Guanajuato México.*
[6] *Fermi National Accelerator Laboratory, Batavia, Illinois 60510, USA*
[7] *University of Rochester, Rochester, New York 14610 USA*
[8] *University of Geneva, Geneva, Switzerland*
[9] *Institute for Nuclear Research of the Russian Academy of Sciences, 117312 Moscow, Russia*
[10] *Centro Brasileiro de Pesquisas Físicas, Rua Dr. Xavier Sigaud 150, Urca, Rio de Janeiro, RJ, 22290-180, Brazil*
[11] *Hampton University, Dept. of Physics, Hampton, Virginia 23668, USA*
[12] *Northwestern University, Evanston, Illinois 60208*
[13] *Department of Physics, University of Minnesota – Duluth, Duluth, Minnesota 55812, USA*
[14] *Universidad Nacional de Ingeniería, Apartado 31139, Lima, Perú*
[15] *Rutgers, The State University of New Jersey, Piscataway, New Jersey 08854, USA*
[16] *Massachusetts College of Liberal Arts, 375 Church Street, North Adams, Massachussetts 01247*
[17] *Departamento de Física, Universidad Técnica Federico Santa María, Avenida España 1680 Casilla 110-V, Valparaíso, Chile*
[18] *University of Florida, Department of Physics, Gainesville, FL 32611*
[19] *Enrico Fermi Institute, University of Chicago, Chicago, Illinois 60637 USA*
[20] *Department of Physics and Astronomy, University of California, Irvine, Irvine, California 92697-4575, USA*
[21] *Department of Physics, Otterbein University, 1 South Grove Street, Westerville, Ohio, 43081 USA*

(Dated: June 25, 2014)

Charged pion production via charged current ν_μ interactions in plastic (CH) is studied using the MINERvA detector exposed to the NuMI wideband neutrino beam at Fermilab. Events with hadronic mass W < 1.4 GeV are selected to isolate single pion production, which is expected to occur primarily through the $\Delta(1232)$ resonance. Cross sections as functions of pion production angle and kinetic energy are reported and compared to predictions from different theoretical calculations and generator-based models, for neutrinos ranging in energy from 1.5 GeV to 10 GeV. The data are best described by calculations which include significant contributions from pion intranuclear rescattering. These measurements constrain the primary interaction rate and the role of final state interactions in pion production, both of which need to be well understood by neutrino oscillation experiments.

PACS numbers: 13.15.+g, 25.80.-e, 13.75.Gx

Introduction–Recent measurements highlight the important role that the nuclear medium plays in the production and propagation of hadrons produced in neutrino-nucleus interactions [1–4]. Experiments find cross section distortions and form-factor modifications which are absent in scattering from free nucleons. This is of particular relevance to neutrino oscillation experiments that make use of nuclear targets such as carbon, oxygen, argon, and iron. In particular, T2K [5] and MiniBooNE [6] rely on the quasielastic interaction on nucleons in oxygen or carbon nuclei, $\nu_\ell N(n) \to \ell^- p$, a relatively well-understood reaction with simple kinematics. The reconstruction and interpretation of events that appear quasielastic are complicated by the presence of the nuclear medium. For example, if a charged-current interaction produces a pion, e.g., $\nu_\ell N(p) \to \ell^- p\pi^+$, and the pion is absorbed by the target nucleus in a Final State Interaction (FSI), the event will appear quasielastic. In such a case, the reconstructed neutrino energy may be significantly underestimated [7], resulting in a bias in the measured oscillation parameters. Neutrino charged-current pion production on heavy nuclei at a few GeV is also an important signal process for current and future long baseline neutrino experiments [8]. Therefore, both pion production and the effect of the nuclear environment on that production must be accurately determined.

In addition to being absorbed, pions may also undergo elastic and inelastic scattering or charge exchange. All of these processes are modeled in neutrino event generators with particle cascade algorithms based on cross section measurements of beam pion absorption [9] or scattering [10] from target nuclei. This technique assumes that interactions of pions created within a nucleus are identical to those of accelerator beam pions, an assumption which is probed by measurements of pion production in electron- and neutrino-scattering experiments.

Electron scattering experiments examine pion production through studies of "color transparency," a process whereby FSI is expected to vanish at high-momentum transfer. These experiments observe a reduction in pion FSI, consistent with Glauber calculations [11]. These measurements, however, are done at higher energies than those of neutrino oscillation experiments; hadronic invariant masses (pion kinetic energies) accessed are greater than 2.1 GeV (3 GeV) [12].

MiniBooNE measures single pion production by neutrinos on mineral oil (CH_2) for $E_\nu \sim 1.0$ GeV, and is sensitive to hadronic invariant masses up to 1.35 GeV and pion kinetic energies from 20 to 400 MeV [13, 14]. The kinetic energy spectra of charged and neutral pions reported by MiniBooNE do not confirm the suppression of high momentum pions predicted by beam-based models of FSI [15–17].

Analysis Strategy–The analysis presented here measures differential cross sections in pion kinetic energy and pion angle in charged-current ν_μ interactions on plastic (CH) at an average neutrino energy of 4.0 GeV [18]. In order to isolate a signal that is dominated by the excitation of the $\Delta(1232)$ P_{33} resonance, the hadronic mass W is required to be less than 1.4 GeV. This allows for a straightforward comparison to theoretical calculations, predictions by neutrino event generators used by oscillation experiments, and the MiniBooNE measurement.

MINERvA Experiment– The MINERvA experiment combines a fine-grained tracking detector [19] with the high-intensity NuMI beam line [20] and the MINOS near detector [21]. The MINERvA detector consists of a central tracking volume of scintillator strips (95% CH and 5% other materials) surrounded by electromagnetic and hadronic calorimeters. Planes of triangular scintillator strips with a 1.7 cm strip-to-strip pitch are arrayed vertically, perpendicular to the horizontal axis (which is inclined by 3.5° relative to the beam direction). Three plane orientations ($0°, \pm 60°$ rotations around the horizontal axis) enable 3-dimensional reconstruction of the neutrino interaction point and the tracks created by outgoing charged particles. The detector's 3.0 ns timing resolution is adequate for separating multiple interactions within a single beam spill. The MINOS near detector, located 2 m downstream of the MINERvA detector, is used to reconstruct muon momentum and charge.

The data for this measurement were taken between March 2010 and April 2012 and represent an integrated 3.04×10^{20} protons on target (POT). For these data the beam line was configured to produce a predominantly muon neutrino beam, and the MINOS detector's polarity was set to focus negative muons.

Experiment Simulations–The neutrino beam is simulated by a Geant4-based model [22, 23] which is constrained to reproduce hadron production measurements by NA49 on carbon [24] and the π/K ratio measured by MIPP on a replica NuMI target [25]. Uncertainty on the neutrino flux is set by the precision in these hadron production measurements, uncertainties in the beam line focusing system and alignment [26], and comparisons between different hadron production models in regions not covered by the NA49 or MIPP data. The integrated neutrino flux over the range $1.5 \leq E_\nu \leq 10.0\,\text{GeV}$ is estimated at $2.77 \times 10^{-8}\,\text{cm}^{-2}/\text{POT}$[1].

Neutrino interactions are simulated using the GENIE 2.6.2 neutrino event generator. Details concerning GENIE, its quasielastic cross section model, and associated parameters are described in Ref [27]. For baryon resonance production, the formalism of Rein-Sehgal [28] is used with modern resonance properties [29]. Nonresonant pion production is simulated using the Bodek-Yang model [30] and is constrained below $W = 1.7$ GeV by neutrino-deuterium bubble chamber data [31, 32].

Pion FSI processes are modeled in GENIE using a simplified intranuclear cascade model which incorporates information from pion-, proton-, and neutron- scattering experiments on nuclei (hA FSI). Uncertainties from the FSI model are evaluated by varying its strength within previously measured uncertainties [10, 33].

The MINERvA detector's response is simulated by a Geant4-based model. The energy scale of the detector is set by requiring agreement between data and simulation of both the photon statistics and the reconstructed energy deposited by momentum-analyzed throughgoing muons. Calorimetric constants used to reconstruct the energy of hadronic showers are determined from the simulation. The uncertainty in the response to single hadrons

[1] See Supplemental Material for the flux as a function of energy.

is constrained by measurements made with a scaled-down replica of the MINERvA detector in a low energy hadron test beam [19]. The response of the MINOS near detector to muons is also simulated by a tuned Geant-based simulation [21].

Event Reconstruction and Selection– Events must contain one muon and at least one hadron track. A negative muon is identified as a track originating in the MINERvA detector that exits the back and can be matched to a negatively charged track observed to enter the upstream planes of MINOS. This is efficient for muon angles with respect to the beam that are less than 20°, and for muon momenta greater than 1.5 GeV. The hadron track(s) of an event must originate from the upstream endpoint of the muon track.

Near the event vertex, individual scintillator strips are often traversed by more than one charged particle. An algorithm is used to divide the energy between the tracks for those cases. To accommodate the strong interactions of the pions within the detector material, the pion tracking algorithm allows for tracks with large-angle scatters. The event vertex, identified by fitting for the intersection of the tracks, is restricted to occur within the central 110 planes of the scintillator tracking region and at least 22 cm from any edge of the planes. These requirements define a fiducial region with a mass of 5.57 metric tons, containing $(3.54 \pm 0.05) \times 10^{30}$ nucleons.

A pion track is identified by the pattern of energy deposition along its length, which differs between charged pions and protons. In addition, the pion track is required to stop in either the tracking or electromagnetic calorimeter regions of MINERvA, which limits the accepted pion kinetic energy to below 350 MeV. Finally, the detection of a Michel electron from the $\pi \to \mu \to e$ decay chain is required, and the efficiency of this selection is validated by comparing stopping muons from upstream neutrino interactions in the data and simulation.

The pion kinetic energy T_π, and angle θ_π are determined by the tracking algorithm. Both W and the square of the four-momentum transfer to the nucleus Q^2 are measured using a calorimetric reconstruction of the energy of final state hadrons E_{had}. All kinematic quantities are then calculated assuming an interaction with a single free nucleon at rest:

$$E_\nu = E_\mu + E_{had}, \tag{1}$$

$$Q^2 = 2E_\nu(E_\mu - |\vec{p}_\mu|cos(\theta_\mu)) - m_\mu^2, \tag{2}$$

$$W^2 = M_p^2 - Q^2 + 2M_p E_{had}. \tag{3}$$

Here, $M_p(m_\mu)$ is the proton (muon) mass; E_μ, p_μ, and θ_μ are respectively the reconstructed energy, momentum, and angle of the muon with respect to the beam. This procedure results in an average W resolution of 6%. To ensure that events with only one charged pion are retained, the analysis only accepts events with W less than 1.4 GeV. The neutrino energy is required to be less than 10 GeV to reduce flux uncertainties. After all cuts, 3474 events remain. The selected pions are predicted to be more than 90% π^+ because of the Michel electron requirement and because π^- can only arise from FSI [16, 34, 35].

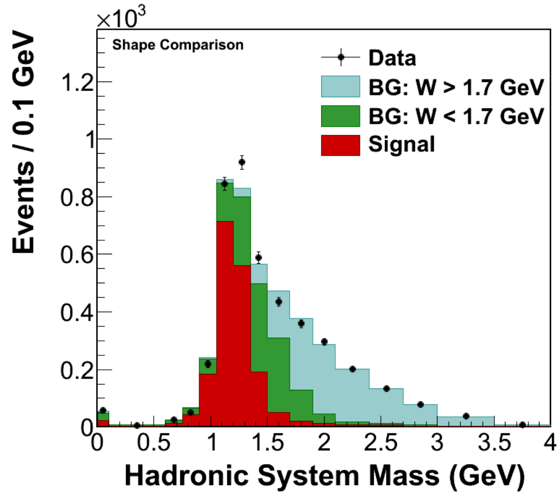

FIG. 1: The reconstructed hadronic system mass (W) distribution for the data (solid circles) and the simulation (histogram) after tuning the background (BG) normalization levels. The signal is defined as $\nu_\mu + N \to \mu^- + \pi^\pm + X$ where the true W is less than 1.4 GeV and the recoil X does not contain additional charged pions. Error bars only include statistical uncertainties.

Cross Section Extraction–To obtain $d\sigma/dT_\pi$ and $d\sigma/d\theta_\pi$ the backgrounds must be subtracted. The largest background to single pion production comes from events at higher W. This background is estimated by creating templates using simulated events for two categories, corresponding to the cases where the true W is either between 1.4 GeV and 1.7 GeV or above 1.7 GeV. Template normalizations are fit to the data for events with a reconstructed W between 0.6 GeV and 2.4 GeV. The W distribution predicted by the simulation after the fit reproduces the data throughout the kinematic sideband region $W > 1.4$ GeV, as shown in Fig. 1. The dominant systematic uncertainty in the background estimate is due to the uncertainty in the detector's calorimetric response model used to reconstruct E_{had}.

The data are then corrected for energy and angular resolution using a Bayesian unfolding method [36]. An underlying Δ decay angular distribution must be assumed in the unfolding and to calculate acceptance: many models assume isotropic decay while Rein-Sehgal predicts a degree of anisotropy [28]. This analysis uses an anisotropy of half that predicted by Rein-Sehgal and excursions from isotropic to the full Rein-Sehgal model are included as systematic uncertainty.

The unfolded event yield is then corrected for detector efficiency and acceptance. Comparisons between data and simulation for test beam pions, muons from upstream neutrino interactions, and neutrino interactions in the detector constrain the uncertainties associated with these corrections. The largest uncertainty in the overall detector efficiency comes from the modeling of the muon angular distribution in resonance production because of the MINOS acceptance. The uncertainty in Δ resonance production is evaluated by varying the neutrino-nucleon cross sections and values of the axial (vector) masses by 20% (50%). The largest systematic uncertainty in the acceptance at low pion kinetic energy comes from the detector mass model uncertainty since a pion must traverse enough planes to be tracked. The largest uncertainty at high pion kinetic energy is from the pion scattering model, which is varied by changing the pion and proton total inelastic cross sections by 10%, corresponding to measured uncertainties [10, 33, 37, 38].

Finally, division of the corrected event yield by the neutrino flux and by the number of target nucleons gives the bin-averaged cross sections. All systematic uncertainties are then evaluated by effecting changes in the simulation and re-extracting the cross section. Since the largest systematic uncertainties are relatively constant and correlated between different T_π or θ_π bins, the shapes of the differential cross sections have significantly lower systematic uncertainties than do the absolute cross sections.

Results– The measured shape of $d\sigma/d\theta_\pi$ is shown in Fig. 2, along with predictions from several models where each model is normalized to the data [2]. The uncertainties on the shape are dominated by the statistical uncertainties. The effect of FSI, shown in the comparison between the GENIE "hA FSI" and "no FSI" curves, is to deplete (increase) some of the forward (backward) angle cross section. The χ^2 between the data and GENIE prediction with (without) FSI is 41 (171) for 12 degrees of freedom, indicating a clear preference for FSI. In particular, the "no FSI" prediction does not describe the relative cross section for backward-going pions.

Predictions from the NuWro [39] and NEUT [40] event generators and a theoretical calculation by Athar, Chaukin, and Singh (ACS) [35] are also shown in Fig. 2. NuWro and NEUT incorporate FSI using microscopic cascade models [41] while the ACS calculation incorporates FSI by applying an attenuation factor as the pion propagates through the nucleus.

The shape of $d\sigma/d\theta_\pi$ could potentially be sensitive to the $\Delta \to \pi$ decay angle distribution. GENIE, GIBUU (shown later), and NuWro use an isotropic decay distribution while NEUT assumes the anisotropy in the Rein-Sehgal model. ACS calculates specific anisotropies for the Δ^{++} and the Δ^{+} separately. The larger effect, however, is the presence or absence of FSI.

[2] See Supplemental Material for the systematic uncertainties in tabular form.

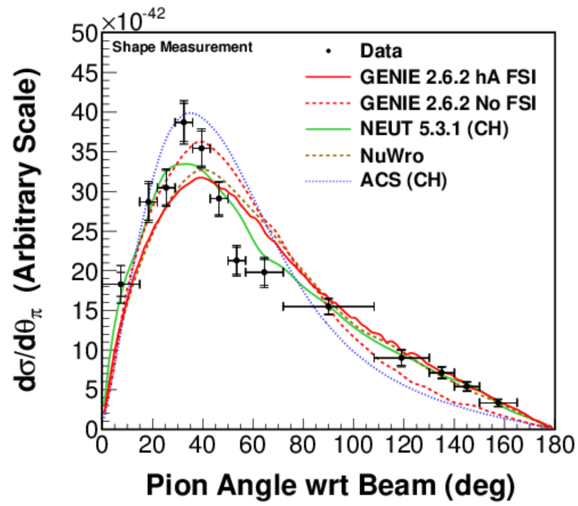

FIG. 2: The measured shape of $d\sigma/d\theta_\pi$ (black circles) compared to GENIE with and without FSI, as well as the ACS, NEUT, and NuWro models, where each prediction is normalized to the data. The inner (outer) error bars correspond to the statistical (total) uncertainties.

T_π (MeV)	I	II	III	IV	V	Total
35 - 55	15 (9.7)	9.7 (2.8)	6.8 (2.9)	8.5 (0.5)	5.5 (2.2)	22 (11)
55 - 75	12 (4.4)	9.7 (3.3)	8.5 (4.4)	8.6 (0.4)	4.8 (1.4)	20 (7.2)
75 - 100	9.9 (4.6)	8.9 (2.3)	6.4 (2.8)	9.0 (0.4)	3.8 (0.6)	18 (5.9)
100 - 125	10 (3.4)	6.8 (1.7)	4.9 (1.4)	9.2 (0.7)	3.0 (0.7)	17 (4.2)
125 - 150	11 (3.0)	6.7 (1.6)	5.0 (1.5)	8.9 (0.2)	3.1 (0.4)	17 (3.7)
150 - 200	11 (3.3)	6.9 (2.2)	3.1 (2.8)	9.1 (0.4)	2.7 (1.6)	16 (5.1)
200 - 350	16 (7.2)	8.5 (1.5)	4.3 (3.1)	9.2 (0.3)	2.9 (1.2)	21 (8.0)

TABLE I: Fractional systematic uncertainties (in per cent) on $d\sigma/dT_\pi$ associated with detector response (I), neutrino cross section model (II), nuclear effects including FSI (III), flux (IV), and other sources (V). The absolute uncertainties are followed by shape uncertainties in parentheses.

The measured $d\sigma/dT_\pi$ is shown in Fig. 3 (top), along with predictions from several models. Table I summarizes the systematic uncertainties on $d\sigma/dT_\pi$. The effects of FSI are again seen in Fig. 3 by comparing the solid and dashed GENIE predictions. The χ^2 between the data and the GENIE model with (without) FSI is 21 (105) for 7 degrees of freedom, again indicating a preference for significant FSI effects.

FSI processes modify the pion production cross section through the peak of the Δ resonance excitation, which in light nuclei occurs at a pion kinetic energy of about 160 MeV. FSI suppresses the cross section for outgoing pions at that energy; pions leave the sample through absorption or charge exchange and migrate to lower energies through scattering. Given the Δ width of 115 MeV [29, 33], this suggests that FSI would create a broad dip in $d\sigma/dT_\pi$ for kinetic energies roughly 100-220 MeV [42].

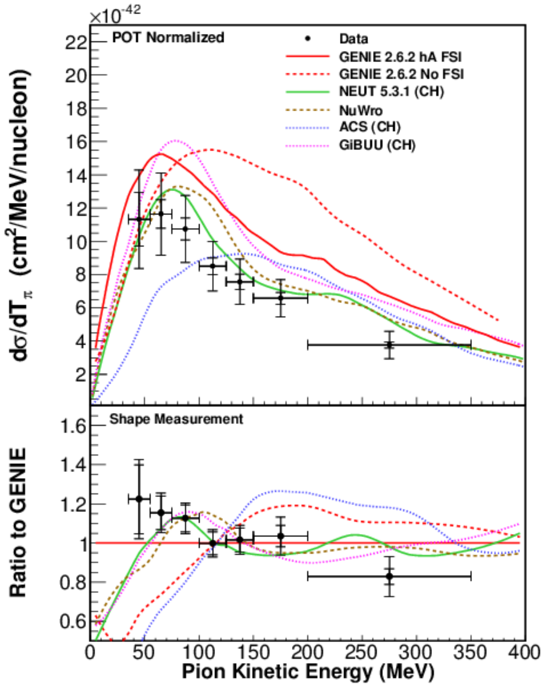

FIG. 3: Top: Measured $d\sigma/dT_\pi$ (black circles) and predictions from GENIE with and without FSI, as well as the ACS, NEUT, GiBUU and NuWro models (curves). The inner (outer) error bars correspond to the statistical (total) uncertainties. The data prefer models that incorporate FSI and a lower integrated cross section than the models. Bottom: Ratio of $d\sigma/dT_\pi$ and predictions to the shape of GENIE with FSI, where all predictions are normalized to the integrated $d\sigma/dT_\pi$ from the data.

Predictions from the NuWro and NEUT event generators and the ACS and GiBUU [34] calculations are shown in Fig. 3. The GiBUU and ACS calculations incorporate nuclear medium effects in Δ production, propagation and non-resonant pion production, while the event generators do not. It is the inclusion of FSI, rather than the incorporation of nuclear medium modifications [15], that most affects the predicted $d\sigma/dT_\pi$ shapes.

The cross section predictions vary significantly because each prediction must reconcile the differences between ANL [43] and BNL [31] bubble chamber measurements of neutrino pion production on deuterium, which differ by 40%. Most models use an average of these two sets of cross sections; the GiBUU model is based upon the BNL cross sections. The POT normalized $d\sigma/dT_\pi$ are in better agreement with models that are based on the ANL data or an average of the two datasets.

Figure 3 (bottom) shows the ratio of the data and several predictions to GENIE with FSI, where all predictions, including GENIE, are normalized to the data. The χ^2 between the data and GENIE prediction with (without) FSI is 7.4 (130) for 6 degrees of freedom. GiBUU, NuWro, and NEUT agree well with the measured shape of $d\sigma/dT_\pi$, while the ACS model is strongly disfavored.

This measurement of $d\sigma/dT_\pi$ is compared with that of MiniBooNE along with the two corresponding GENIE predictions with FSI for the appropriate neutrino fluxes [44] in Fig. 4. MINERvA measures higher energy and higher Q^2 neutrino interactions than does MiniBooNE, but the W regions and pion kinetic energies in the two experiments overlap. The contributions due to Δ excitation and the non-resonant backgrounds differ, but the key feature of attenuation due to pion FSI is expected to be similar. Both the MINERvA and MiniBooNE results have similar shapes monotonically decreasing above $T_\pi = 100$ MeV. The GENIE model with FSI predicts the shape but overpredicts the level of the MINERvA data, while it predicts the rate but not the shape of the MiniBooNE data [17]. The same trend is seen with the GiBUU calculation, as shown in Fig. 3 and Ref. [15].

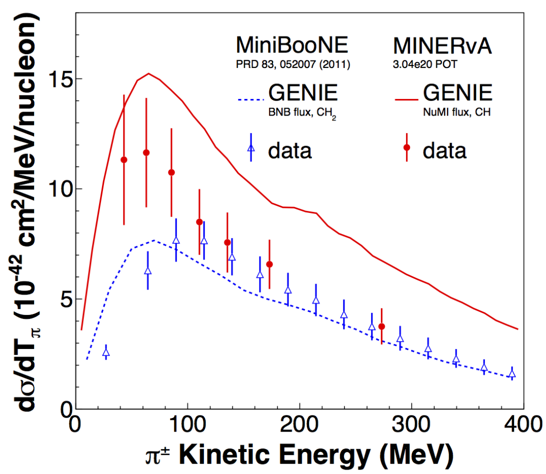

FIG. 4: $d\sigma/dT_\pi$ comparison between the MINERvA data (circles) and GENIE 2.6.2 "hA FSI" prediction for NuMI (solid curve) along with the MiniBooNE π^+ data [13] (triangles) and the corresponding prediction (dashed curve). Error bars indicate the total uncertainty in each measurement.

Conclusions– This letter presents measurements of neutrino-induced pion production from a CH target and compares them to models with different FSI treatments and to MiniBooNE. Both the $d\sigma/d\theta_\pi$ and $d\sigma/dT_\pi$ shapes strongly favor models with FSI. These data place strong constraints on FSI and provide new information about the neutrino energy dependence. These measurements may help resolve a long-standing discrepancy between neutrino-induced pion production measurements on deuterium from ANL and BNL bubble chambers. More generally, they provide an observational foundation for improving both the background and signal predictions needed for precise oscillation parameter measurements in the few GeV regime.

This work was supported by the Fermi National Accelerator Laboratory under U.S. Department of Energy Contract No. DE-AC02-07CH11359 which included the

MINERvA construction project. Construction support also was granted by the United States National Science Foundation under Grant No. PHY-0619727 and by the University of Rochester. Support for participating scientists was provided by NSF and DOE (USA) by CAPES and CNPq (Brazil), by CoNaCyT (Mexico), by CONICYT (Chile), by CONCYTEC, DGI-PUCP and IDI/IGI-UNI (Peru), by Latin American Center for Physics (CLAF), by the Swiss National Science Foundation, and by RAS and the Russian Ministry of Education and Science (Russia). We thank the MINOS Collaboration for use of its near detector data. Finally, we thank the staff of Fermilab for support of the beam line and detector.

---

* now at SLAC National Accelerator Laboratory, Stanford, California 94309 USA

† also at Department of Physics, University of Antananarivo, Madagascar

‡ also at Institute of Theoretical Physics, Wrocław University, Wrocław, Poland

§ now at Argonne National Laboratory, Argonne, Illinois 60439, USA

[1] G. Fiorentini *et al.* (MINERvA Collaboration), Phys. Rev. Lett. **111**, 022502 (2013).

[2] L. Fields *et al.* (MINERvA Collaboration), Phys. Rev. Lett. **111**, 022501 (2013).

[3] A. A. Aguilar-Arevalo *et al.* (MiniBooNE Collaboration), Phys. Rev. Lett. **100**, 032301 (2008).

[4] A. A. Aguilar-Arevalo *et al.* (MiniBooNE Collaboration), Phys. Rev. D **88**, 032001 (2013).

[5] K. Abe *et al.* (T2K Collaboration), Phys. Rev. Lett. **112**, 061802 (2014).

[6] A. A. Aguilar-Arevalo *et al.* (MiniBooNE Collaboration), Phys. Rev. Lett. **105**, 181801 (2010).

[7] O. Lalakulich, U. Mosel, and K. Gallmeister, Phys. Rev. C **86**, 054606 (2012).

[8] T. Akiri *et al.* (LBNE Collaboration), (2011), arXiv:1110.6249 [hep-ex] .

[9] D. Ashery and J. Schiffer, Ann. Rev. Nucl. Part. Sci. **36**, 207 (1986).

[10] T. Lee and R. Redwine, Ann. Rev. Nucl. Part. Sci. **52**, 23 (2002).

[11] W. Cosyn, M.C. Martinez, J. Ryckebusch, and B. Van Overmeire, Phys. Rev. C **74**, 062201 (2006).

[12] X. Qian, T. Horn, B. Clasie, J. Arrington, R. Asaturyan, *et al.*, Phys. Rev. C **81**, 055209 (2010).

[13] A.A. Aguilar-Arevalo *et al.* (MiniBooNE Collaboration), Phys. Rev. D **83**, 052007 (2011).

[14] Y. Kurimoto *et al.* (SciBooNE Collaboration), Phys. Rev. D **81**, 033004 (2010).

[15] O. Lalakulich and U. Mosel, Phys. Rev. C **87**, 014602 (2013).

[16] E. Hernández, J. Nieves, and M.J. Vicente Vacas, Phys. Rev. D **87**, 113009 (2013).

[17] P. Rodrigues, (2014), arXiv:1402.4709 [hep-ex] .

[18] B. Eberly, *Characterization of Final State Interaction Strength in Plastic Scintillator by Muon-Neutrino Charged Current Charged Pion Production*, Ph.D. thesis, Univ. of Pittsburgh (2014).

[19] L. Aliaga *et al.* (MINERvA Collaboration), Nucl. Instrum. Methods in Phys. Res., Sect. A **743**, 130 (2014).

[20] K. Anderson, B. Bernstein, D. Boehnlein, K. R. Bourkland, S. Childress, *et al.*, *The NuMI Facility Technical Design Report*, FERMILAB-DESIGN-1998-01 (1998).

[21] D. G. Michael *et al.* (MINOS Collaboration), Nucl. Instrum. Methods Phys. Res., Sect. A **596**, 190 (2008).

[22] S. Agostinelli *et al.*, Nucl. Instrum. Methods Phys. Res., Sect. A **506**, 250 (2003).

[23] J. Allison *et al.*, Nuclear Science, IEEE Transactions on **53**, 270 (2006).

[24] C. Alt *et al.* (NA49 Collaboration), Eur. Phys. J. C **49**, 897 (2007).

[25] A. V. Lebedev, *Ratio of pion kaon production in proton carbon interactions*, Ph.D. thesis, Harvard University (2007).

[26] Z. Pavlovic, *Observation of Disappearance of Muon Neutrinos in the NuMI Beam*, Ph.D. thesis, University of Texas (2008).

[27] C. Andreopoulos, A. Bell, D. Bhattacharya, F. Cavanna, J. Dobson, *et al.*, Nucl. Instrum. Methods Phys. Res., Sect. A **A614**, 87 (2010), Program release 2.6.2 used here.

[28] D. Rein and L. M. Sehgal, Ann. Phys. **133**, 79 (1981).

[29] J. Beringer *et al.* (Particle Data Group), Phys. Rev. D **86**, 010001 (2012).

[30] A. Bodek, I. Park, and U.-K. Yang, Nucl. Phys. Proc. Suppl. **139**, 113 (2005).

[31] G. Radecky *et al.*, Phys. Rev. D **25**, 1161 (1982).

[32] T. Kitagaki, H. Yuta, S. Tanaka, A. Yamaguchi, K. Abe, *et al.*, Phys. Rev. D **42**, 1331 (1990).

[33] D. Ashery, I. Navon, G. Azuelos, H. Walter, H. Pfeiffer, *et al.*, Phys. Rev. C **23**, 2173 (1981).

[34] U. Mosel, O. Lalakulich, and K. Gallmeister, Phys. Rev. D **89**, 093003 (2014).

[35] M.S. Athar, S. Chauhan, and S.K. Singh, Eur. Phys. J. A **43**, 209 (2010).

[36] G. D'Agostini, Nucl. Instrum. Methods Phys. Res., Sect. A **362**, 487 (1995).

[37] B. Allardyce, C. Batty, D. Baugh, E. Friedman, G. Heymann, *et al.*, Nucl. Phys. **A209**, 1 (1973).

[38] A. Saunders, S. Hoeibraten, J. Kraushaar, B. Kriss, R. Peterson, *et al.*, Phys. Rev. C **53**, 1745 (1996).

[39] T. Golan, C. Juszczak, and J. T. Sobczyk, Phys. Rev. C **86**, 015505 (2012).

[40] Y. Hayato, Acta Phys. Polon. B **40**, 2477 (2009).

[41] M. Vicente Vacas, M. Khankhasaev, and S. Mashnik, (1994), arXiv:nucl-th/9412023 .

[42] T. Leitner, O. Buss, U. Mosel, and L. Alvarez-Ruso, Phys. Rev. C **79**, 038501 (2009).

[43] T. Kitagaki *et al.*, Phys. Rev. D **34**, 2554 (1986).

[44] A. Aguilar-Arevalo *et al.* (MiniBooNE Collaboration), Phys. Rev. D **79**, 072002 (2009).